

The human inferior parietal cortex: Cytoarchitectonic parcellation and interindividual variability

Svenja Caspers,^a Stefan Geyer,^{a,b} Axel Schleicher,^a Hartmut Mohlberg,^b Katrin Amunts,^b and Karl Zilles^{a,b,*}

^aC. and O. Vogt Brain Research Institute, University of Düsseldorf, P.O. Box 10 10 07, 40001 Düsseldorf, Germany

^bInstitute of Medicine, Research Center Jülich, 52425 Jülich, Germany

Received 16 March 2006; revised 19 June 2006; accepted 20 June 2006

Available online 1 September 2006

The inferior parietal cortex (IPC) integrates information from different sensory modalities and plays an important role in a variety of higher cognitive functions. Brodmann (Brodmann, K., 1909. Vergleichende Lokalisationslehre der Großhirnrinde. Barth, Leipzig) proposed a cytoarchitectonic subdivision of the IPC into only two cortical areas, a rostral (BA 40) and a caudal (BA 39) area. Although his scheme was repeatedly challenged by other observers, it is still used for the anatomical localization of functional imaging data. The apparent differences between all these cyto- and myeloarchitectonic maps may be caused partly by the observer-dependent procedure of defining cytoarchitectonic borders by pure visual inspection of histological sections and partly by the interindividual variability of cytoarchitecture. The present observations and the resulting cortical map of the IPC are based on quantitative, observer-independent definitions of cytoarchitectonic borders and take into account each area's topographical variability across brains. Ten human postmortem brains were scanned using an MRI 3-D FLASH sequence prior to histological processing. After embedding in paraffin, serial sections through whole brains were prepared, and the sections were stained for cell bodies. Following high-resolution digitization of sections containing the IPC, we defined the cytoarchitecture and borders of each cortical area of this brain region using a multivariate statistical analysis of laminar cell density profiles. In contrast to previous observations, we found seven cytoarchitectonic areas in the IPC: five in the rostral (covering the region of BA 40) and two in the caudal part (covering the region of BA 39). We observed considerable interindividual variability in the topography of each area. A consistent correspondence between macroanatomical landmarks and cytoarchitectonic borders was not found. This new cytoarchitectonic map of the human IPC demonstrates regional differences in the cortical microstructure that is suggestive of functional differentiation. Furthermore, the map is registered in

three dimensions and thereby provides a robust anatomical base for interpreting functional imaging studies.

© 2006 Elsevier Inc. All rights reserved.

Keywords: Parietal cortex; Cytoarchitecture; Brain mapping; Interindividual variability

Introduction

The inferior parietal cortex (IPC) integrates various modalities (e.g., somatosensory, visual, and auditory) and plays an important role in various higher cognitive functions. One may wonder whether this functional complexity is reflected at a structural (e.g., cytoarchitectonic) level.

According to Brodmann (1909; Fig. 1A), the IPC consists of two different cytoarchitectonic areas: BA 40 located on the supramarginal gyrus and BA 39 on the angular gyrus. Rostrally, BA 40 borders the somatosensory cortex (BA 2). Ventrally, BA 40 reaches into the depth of the operculum Rolandi and dorsally to the intraparietal sulcus. The ventral part of BA 39 abuts the temporal cortex. The caudal part of BA 39 borders the occipital cortex.

Other cyto- or myeloarchitectonic maps of this cortical region have been published by Campbell (1905), Vogt and Vogt (1919; Fig. 1B), von Economo and Koskinas (1925; Figs. 1C and D), Gerhardt (1940), Bailey and von Bonin (1951), Sarkissov et al. (1955; Fig. 1E), and Batsch (1956). None of these maps, however, takes into account the interindividual variability of the cortical areas, especially with respect to size and their positions relative to macroscopical landmarks. Furthermore, the maps were published as schematic drawings. Thus, a volume or surface based reference system, which provides the opportunity to import and spatially normalize structural or functional data from other brains, is missing. A third problem is the observer-dependent method of classical cytoarchitectonic studies. As a consequence, the maps are

* Corresponding author. C. und O. Vogt Brain Research Institute, Universitätsstr. 1, 40225 Düsseldorf, Germany. Fax: +49 211 81 12336.

E-mail address: zilles@hira.uni-duesseldorf.de (K. Zilles).

Available online on ScienceDirect (www.sciencedirect.com).

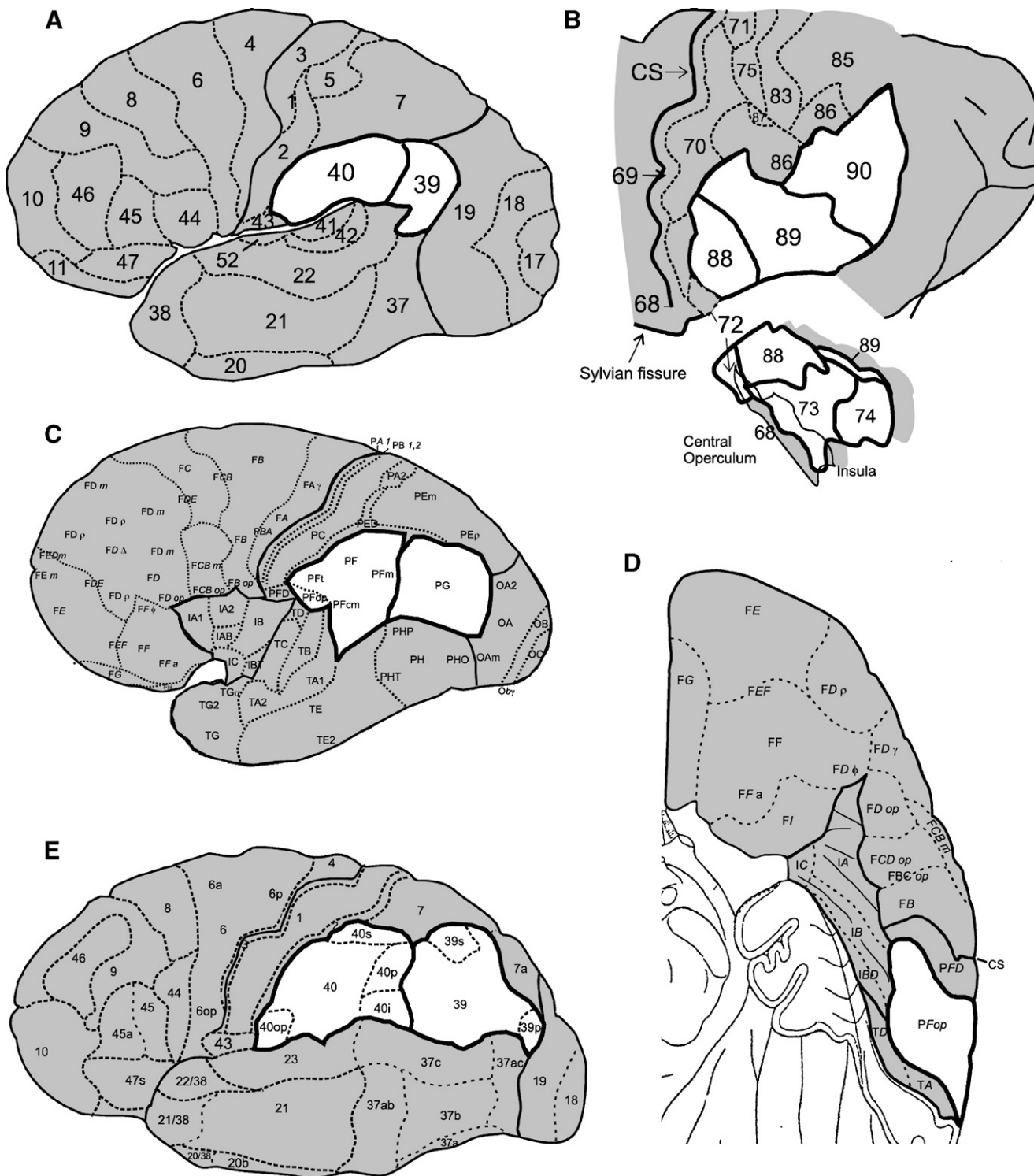


Fig. 1. Schematic drawings of the “classical” brain maps of (A) Brodmann (1909), (B) Vogt and Vogt (1919; inset: ventral view of the parietal operculum; CS: central sulcus), (C, D) von Economo and Koskinas (1925; C: lateral view; D: ventral view with temporal lobe removed), and (E) Sarkissov et al. (1955). Areas of the IPC are highlighted.

strongly influenced by each investigator’s criteria for defining microstructural borders between cortical areas. This led to considerable differences between the maps. For example, in sharp contrast to Brodmann (1909), von Economo and Koskinas (1925) subdivided BA 40 into five areas.

In the present study, the borders of cytoarchitectonic areas were delineated in 10 postmortem brains using an observer-independent technique (Schleicher et al., 1999; Zilles et al., 2002). The brains and areas were then spatially normalized to the Montreal Neurological Institute (MNI) single reference brain, and a

probability map was generated for each area by superimposing the data from all ten brains. An area's probability map reflects the interindividual variability of this area with respect to size and location since a single voxel in MNI space represents the frequency of the representation of parts of this particular area found in one up to ten brains. Following normalization, the 3-D cytoarchitectonic probability maps can be co-registered and compared with functional MRI or PET data in the same reference space (Eickhoff et al., 2005).

This probabilistic and observer-independent procedures have already successfully applied in studies of the somatosensory (BA 3a, 3b, 1; Geyer et al., 1999; BA 2: Grefkes et al., 2001), motor (BA 4: Geyer et al., 1996), and premotor cortex (BA 6: Geyer, 2004), Broca's speech region (BA 44 and 45: Amunts et al., 1999), primary auditory cortex (BA 41: Morosan et al., 2001), visual cortex (BA 17 and 18: Amunts et al., 2000), and, most recently, the parietal operculum (Eickhoff et al., 2006a,b) and areas hIP1 and hIP2 in the intraparietal sulcus (Choi et al., 2006).

In the present study, we used the same methodical approach to study the cytoarchitectonic organization of the IPC. We found a mosaic of seven areas: five are located on the supramarginal gyrus, two lie on the angular gyrus.

Materials and methods

Histology and MR scanning of postmortem brains

We analyzed ten postmortem brains (5 males, 5 females, ranging in age from 37 to 86 years, cf. Table 1) obtained through the body donor program of the Department of Anatomy, University of Düsseldorf, Germany. Subjects had no known history of neurological or psychiatric diseases. We removed the brains from the skull and fixed them for approximately 5 months in 4% formaldehyde diluted in water or in Bodian's fixative (90 ml of 80% ethanol, 5 ml of 37% formaldehyde diluted in water, and 5 ml of glacial acetic acid). During fixation, the brains were suspended on the basilar artery to avoid compression or distortions. After fixation, we scanned each brain with a T1-weighted MR sequence (1.5 T Siemens Magnetom SP scanner, 3-D fast low angle shot (3-D FLASH) pulse sequence, flip angle=40°, TR=40 ms, TE=5 ms, voxel size=1.17 mm (x)×1 mm (y)×1 mm (z)) in order to document brain size and shape before subsequent histological processing. We dehydrated the brains in graded alcohols, embedded them in paraffin, and sectioned them in a coronal plane using a large-scale microtome (20 μm thick serial whole-brain sections, Fig. 2A). While sectioning the brain, we obtained blockface images after each 60th section with a CCD camera (XC-75, Sony, Japan, image matrix=256×256 pixels, 8 bit gray value resolution). We mounted each 60th section on a gelatin-coated slide and stained it for cell bodies with a modified silver

Table 1
Brains used for cytoarchitectonic analysis of the inferior parietal cortex

Brain no.	Sex	Age	Cause of death	Fixative
14/94	Female	43	Pulmonary embolism	Formalin
16/96	Male	54	Myocardial infarction	Formalin
139/95	Male	74	Myocardial infarction	Formalin
146/86	Male	37	Right heart failure	Formalin
2/95	Female	85	Mesenteric artery infarction	Bodian
207/84	Male	75	Toxic glomerulonephritis	Formalin
2431	Male	39	Drowning	Formalin
382/81	Female	59	Cardiorespiratory failure	Formalin
68/95	Female	79	Cardiorespiratory failure	Bodian
71/86	Female	86	Cardiorespiratory failure	Formalin

method (Merker, 1983) for observer-independent cytoarchitectonic analysis (Fig. 2B).

Observer-independent delineation of cytoarchitectonic borders

In each cell-stained section, we defined a rectangular region of interest (ROI) which encompassed the supramarginal or angular gyrus (Fig. 2B) and scanned each ROI in a meander-like sequence with a CCD camera (XC-75, Sony, Japan) and a microscope (Universal, Zeiss, Germany) equipped with a computer-controlled motorized stage. The obtained images (736×544 μm each) of a ROI were further processed with an image analysis software package (KS 400, Zeiss, Germany) to determine the volume fraction of darkly stained cell bodies (gray level index GLI) after adaptive thresholding (Schleicher and Zilles, 1990). GLI values were measured in square, adjacent measuring fields, each 16×16 μm wide. The final data matrix covering the entire ROI is visualized as a GLI image (Fig. 2C). For further details, see Schleicher and Zilles (1990) and Zilles et al. (2002).

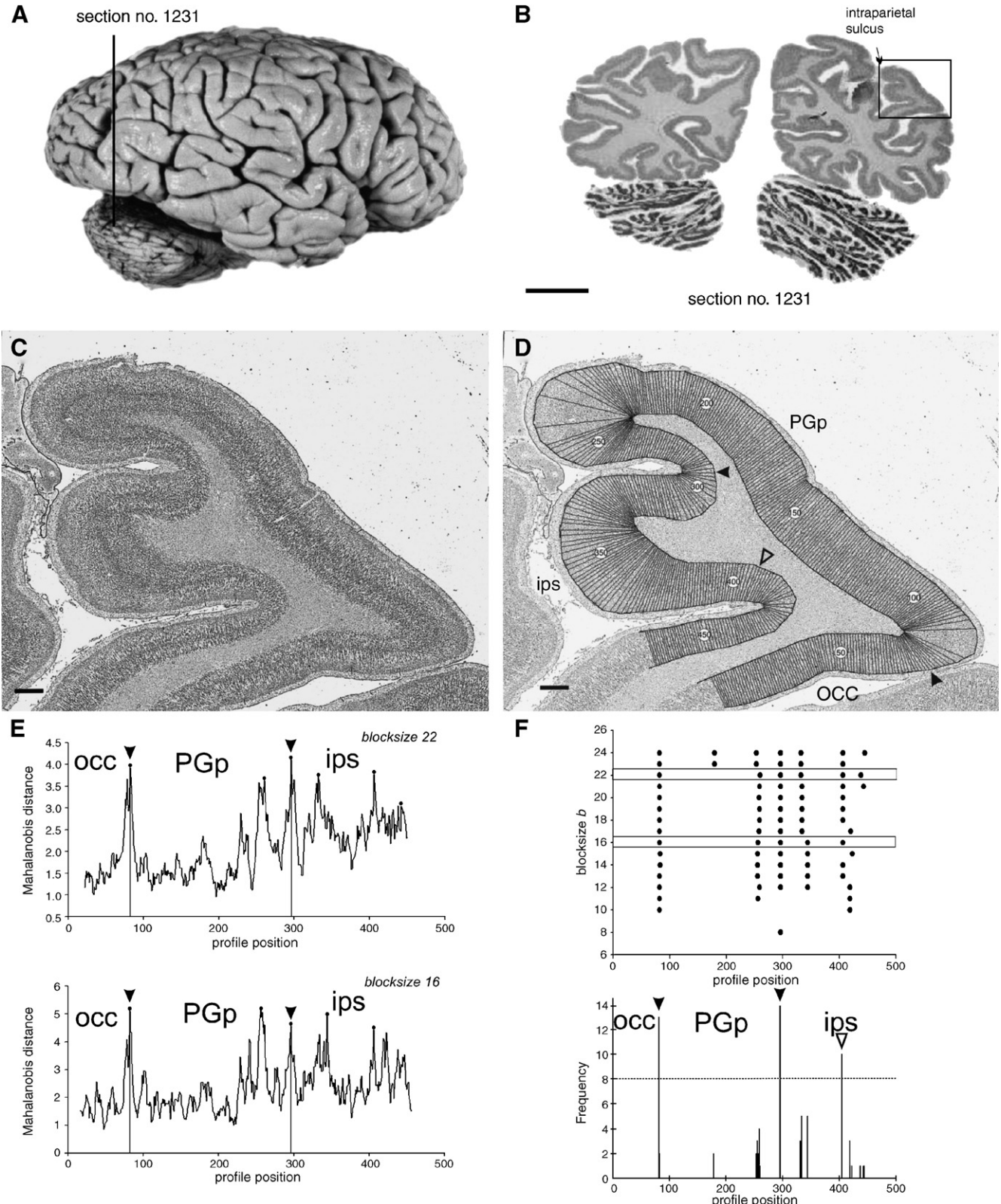
From each GLI image, we extracted GLI profiles running perpendicularly to the cortical layers. To this end, we interactively drew outer (between layer I and II) and inner (between layer VI and the white matter) contour lines of the cerebral cortex using a MATLAB (The MathWorks, Inc., Natick, MA, USA) routine. We then extracted GLI profiles using a physical model based on electric field lines extending between the outer and inner contour line (Jones et al., 2000). We defined linear traverses by connecting the start-and end-point of each field line (Schmitt and Böhme, 2002, 2003; Fig. 2D) and, along each traverse, extracted the GLI values from the digitized image. To compensate for variations in cortical thickness, we resampled each profile with linear interpolation to a standard length corresponding to a cortical thickness of 100%.

To quantify each profile's shape, we extracted five features based on central moments (mean y (y =GLI), mean x (x =cortical depth), standard deviation of x , skewness, and kurtosis) from (i) the

Fig. 2. Example of the observer-independent mapping procedure. (A) Right lateral view of one of the ten brains (vertical line indicates position of histological section no. 1231). (B) Coronal whole-brain section no. 1231 (cell body stained) with ROI (box) to be analyzed for areal borders. Scale bar: 20 mm. (C) GLI image of the ROI (dark pixels correspond to high, bright pixels to low volume fractions of cell bodies). Scale bar: 1 mm. (D) GLI image of this ROI with outer and inner contour lines and positions of 472 GLI profiles superimposed. Arabic numerals indicate each 50th profile. Arrowheads mark the borders of area PGp to the occipital cortex (occ, right arrowhead) and the intraparietal sulcus (ips, left arrowhead). An additional, light arrowhead marks a border of a presently unidentified area in the ips. Scale bar: 1 mm. (E) Mahalanobis distance functions (ordinate) plotted against profile positions (abscissa) for blocksize b =16 (bottom) and b =22 (top). Significant maxima are marked with asterisks and the corresponding borders shown in D with arrowheads and vertical lines. (F) Top: Positions of significant maxima (abscissa) plotted against blocksize b (ordinate). Horizontal frames at b =16 and b =22 correspond to Mahalanobis distance functions in E. Bottom: Frequency of significant maxima (ordinate) of the graph above against profile position. In this example, profile positions with frequencies above 8 (dashed horizontal line, near to half of the maximally possible frequency of 17) are accepted as anatomical borders (for further details, see text).

profile and (ii) the absolute value of its first derivative. We combined the ten feature values into one feature vector X . In a next step, a mean feature vector X_1 from a set (block) of b adjacent profiles ($8 \leq b \leq 24$), and another mean feature vector X_2 from a neighboring block of b adjacent profiles ($8 \leq b \leq 24$) were

calculated. The number of profiles per block (b) defines the spatial resolution of this procedure; that is, only cytoarchitectonic entities wider than the cortical sector sampled by one block of profiles can be detected. The Mahalanobis distance (Mahalanobis et al., 1949) was determined for each combination of mean vectors X_1, X_2 using



a sliding window technique and plotted as a function of the positions of the border between these profile blocks with respect to the cortical ribbon. The Mahalanobis distance function showed maxima at those positions in the cortex where the profiles maximally differed in shape representing the laminar distribution of GLIs. We tested these maxima for statistical significance with a Hotelling's T^2 test and Bonferroni correction for multiple comparisons (Fig. 2E). For further details, see Schleicher et al. (1999) and Zilles et al. (2002). In most cases, we calculated the distance functions for block sizes of $b=8$ to $b=24$ (b =number of profiles per block) in each ROI and plotted the positions of significant maxima as a function of b (Fig. 2F). The frequency of maxima at comparable positions was used to define putative thresholds adequate for detecting the specific cytoarchitectonic differences between the actual areas under investigation. This threshold sets the sensitivity for detecting borders; it has to be adjusted to the actual cytoarchitectonic composition of a section. In a few instances (cf. Fig. 7C—border between PFcm and PFop), however, the cytoarchitectonic patterns of two adjacent areas (as quantified by the GLI profiles) differed only slightly between the areas. Obviously, in this setting, high frequencies of maxima could be caused by artifacts, i.e., tissue damage or tangential sectioning. The relevant cytoarchitectonic border on the other hand will only be reflected by lower maxima frequencies. The threshold for partitioning the cortical stripe thus had to be adjusted to lower levels than $b=8$. In contrast, other borders under investigation like the one between PGp and the occipital lobe (Fig. 12B) were much better detectable, resulting in a considerably higher frequency of maxima at these positions. Such borders could, therefore, be confirmed at higher frequency levels. This dynamical adaptation of the cut-off frequency was crucial to ensure sufficient sensitivity of the quantitative cytoarchitectonic analysis, while avoiding or disregarding false positive parcellations. The location of each putative border was then followed up through stacks of neighboring sections, and only those borders that could be traced in a continuous representation across space were considered in the anatomical parcellation of the IPC. Finally, the hereby defined architectonic entities were compared with the original histological sections by microscopical inspection for the description of cellular characteristics as well as identification of cytoarchitectural features and assignments as described in the literature.

3-D reconstruction of postmortem brains

To display the topography of each area on its brain's cortical surface, we digitized each cell-stained section with a CCD camera (XC-75, Sony, Japan). We reconstructed each postmortem brain in 3-D (Schormann and Zilles, 1998) from (i) the images of the paraffin blockface, (ii) the digitized histological sections, and (iii) the brain's T1-weighted MR scan. Since the MR scan was obtained prior to histological processing, artefacts (e.g., shrinkage of the brain due to dehydration in graded alcohols, embedding in paraffin, distortion of the sections due to cutting) could be eliminated in the reconstructed volume by matching it with the MR volume of the same brain and using linear and nonlinear correction procedures. We labeled each area in the coronal sections of the reconstructed volume according to the area's topography in the corresponding cell-stained sections (Amunts et al., 1999, 2000; Eickhoff et al., 2006a,b; Geyer et al., 1999; Geyer et al., 1996; Geyer, 2004; Grefkes et al., 2001; Morosan et al., 2001). After smoothing with an isotropic Gaussian kernel (full-width half-maximum (FWHM)=1.2 mm), we rendered each brain's surface and IPC areas.

Results

The observer-independent mapping procedure

An example of the observer-independent procedure will be given here in some detail to illustrate the cytoarchitectonic mapping method used in the present study. Fig. 2A shows a lateral view of one of the ten brains after fixation. A coronal whole-brain section no. 1231 (cf. vertical line in Fig. 2A) through this brain, stained for cell bodies, is depicted in Fig. 2B. The box in Fig. 2B marks the ROI within which GLI profiles were extracted. The GLI image of this ROI is depicted at higher magnification in Fig. 2C. In the GLI image, we interactively draw an outer (between layer I and II) and inner (between layer VI and the white matter) contour line and extracted GLI profiles running perpendicularly to the cortical layers (Fig. 2D). The Mahalanobis distances are plotted for two different block sizes ($b=16$ GLI profiles (bottom) and $b=22$ GLI profiles (top)) as functions of their positions along the cortical ribbon (Fig. 2E). Statistically significant maxima are marked with black asterisks. Fig. 2F (top) shows the effect of increasing values of b by processing the same set of profiles (cf. Fig. 2D) for $b=8$ to $b=24$. Only the positions of significant maxima are indicated (horizontal frames at $b=16$ and $b=22$ correspond to Mahalanobis curves in Fig. 2E bottom and top, respectively). Smoothing of the distance functions increases with higher values of b , but the positions of the maxima remain remarkably stable. The positions of cytoarchitectonically meaningful maxima are confirmed by plotting the absolute frequencies of the significant maxima (ordinate) against the profile position (abscissa). In this example, those profile positions where significant maxima occurred with frequencies above eight (dashed horizontal line in Fig. 2F, bottom) were accepted as borders. This threshold above eight sets the sensitivity of the mapping procedure with respect to the number of borders detected. The threshold was determined in such a way that comparable positions of the resulting borders must be identifiable across stacks of neighboring sections (criterion of anatomical consistency). This allows to minimize the detection of false positive "borders", i.e., borders found in only one section. It is not an absolute threshold generally applicable throughout the whole human neocortex, but has to be slightly adjusted to the contrast in cytoarchitecture between the actual areas under investigation (Figs. 7–12). For details, see Zilles et al. (2002).

In the example given in Fig. 2, borders are located at profile positions 78, 296, and 406. These observer-independently identified areas and their borders (marked in Fig. 2D) were subsequently studied by microscopical inspection of the cytoarchitectonical pattern in the histological sections. The border at profile position 78 coincides with the cytoarchitectonical border between area PGp and the adjoining occipital cortex (occ), the border at profile position 296 coincides with the border between PGp and the intraparietal sulcus (ips), and the border at profile position 406 is located within the ips.

Cytoarchitectonic features of the IPC areas

Based on the above described procedure, we defined a mosaic of seven regions in the IPC. Five regions are located on the supramarginal gyrus (approximately in the region of BA 40), the other two regions are found on the angular gyrus (approximately in the region of BA 39). As far as possible, we adopted the

nomenclature of von Economo and Koskinas (1925; cf. Figs. 1C and D). The five regions PF, PFcm, PFm, PFop, and PFt of the supramarginal gyrus are arranged in two rostro-caudal rows: a dorsal row with three regions and a ventral row with two smaller regions. On the angular gyrus, where both Brodmann (1909) and von Economo and Koskinas (1925) found only one region (BA 39 and area PG, respectively), we discerned one rostral (PGa) and one caudal region (PGp).

Area PFop is located rostro-ventrally in the IPC. Its cytoarchitectonic pattern is very homogeneous (Fig. 3A). The cortical layers are poorly separated, and the sizes of the pyramidal cells do not vary much among the different layers. The cell density in layer II is relatively low. There is a superficial-to-deep increase in the size of pyramidal cells in layer III. Layer IIIc pyramids are larger than those of layer V. Layer IV is sparsely developed, and layer V cannot be subdivided into an upper and lower part. The border between layer VI and the white matter is clearly visible.

Area PFt lies dorsal to PFop. Its cortical layers are separated more clearly than those in PFop (Fig. 3B). Layer II of PFt has a higher cell density than that of PFop. The large pyramidal cells of lower layer III are prominent. The pyramids of layer III also

increase in size from superficial to deeper parts. The pyramids in layer IIIc are larger than those of layer V and define a sharp border with layer IV. Although layer IV stands out more clearly than it does in PFop, it is also rather thin. Layer V can be subdivided into a superficial part (layer Va) with higher cell density and a deeper part (layer Vb) with lower cell density. Layer VI is clearly visible, having sharp borders with layer Vb and the white matter.

Area PF, the largest region of the IPC, lies caudal to PFt. PF is very broad, and all its layers are cell dense (Fig. 4A). Layer II is poorly separated from upper layer III because the granular cells of layer II intermingle with the small pyramids in upper layer III. Layer III represents the major part of the cortical width; its pyramidal cells have a marked superficial-to-deep increase in size. The pyramidal cells of layer IIIc are larger than those of layer V. Layer IV is clearly visible but is interrupted by vertical strands of pyramidal cells which extend from deep layer III to upper layer V (arrows in Fig. 4A). This feature leads to the impression that layer IV consists of clusters of granular cells. The medium-sized pyramids in layer V are evenly distributed and no sub-layers are observed. The border between layer V and VI is difficult to recognize. The border between layer VI and the white matter is not

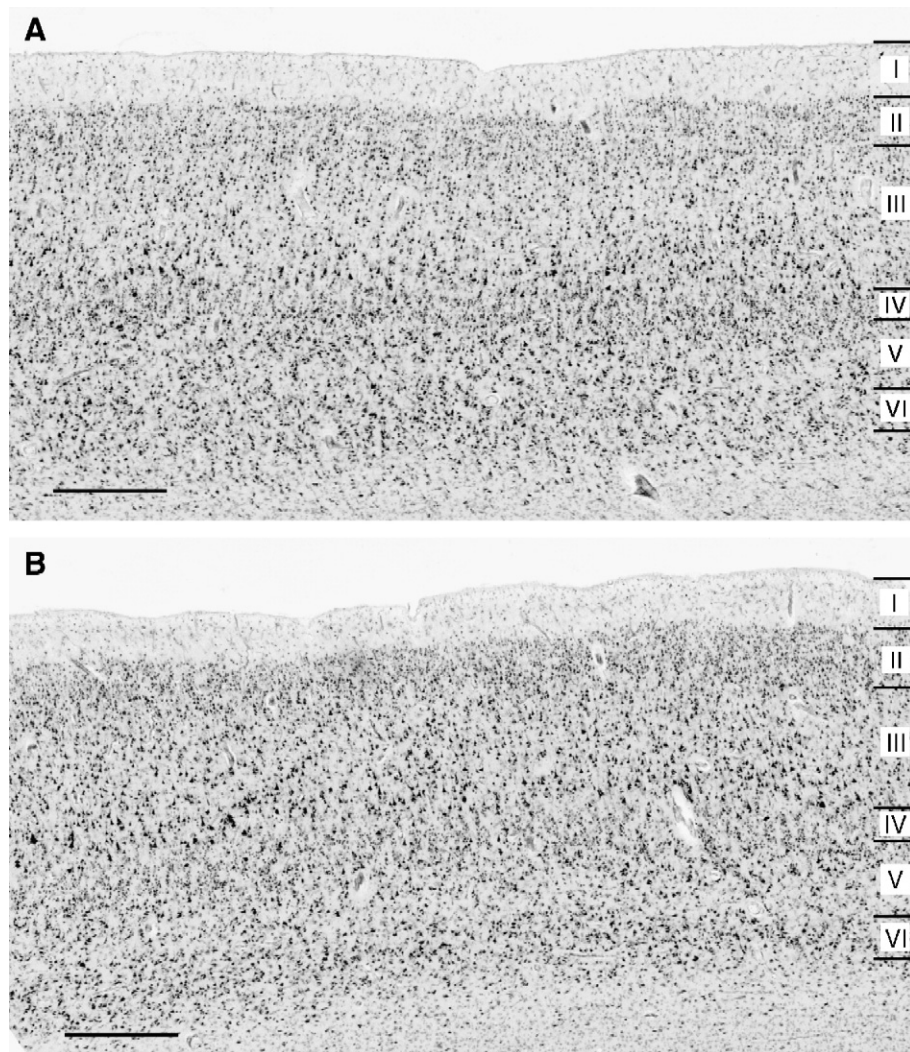


Fig. 3. (A) Cytoarchitecture of area PFop. (B) Cytoarchitecture of area PFt. Roman numerals indicate cortical layers. Scale bar (A, B): 500 µm.

as sharp as it is in areas PFop or PFt. The cells in layers IIIb through VI exhibit a moderate columnar arrangement.

Area PFm (Fig. 4B) abuts caudally on area PF. The cytoarchitectonic features of the anterior and posterior IPC merge in area PFm: it may be interpreted as a transition zone between the two cortical regions, PF and PG. The cortex of PFm is very broad, as in area PF. Likewise, the border between layers II and III is difficult to detect. The pyramids show a pronounced superficial-to-deep increase in size across layer III; layer IIIc pyramids of PFm are larger than those in area PF. The cells in layers IIIb to VI of PFm are arranged in columns. Layer IV is more clearly separated from layers III and V than anywhere else in the PF region. A well demarcated layer IV can also be found in the PG region. This common feature suggests that area PFm is a transition zone between rostral and caudal regions of IPC. Another common feature is the low cell density and small size of the pyramids in layer V. It gives the impression of a light layer V, especially in contrast to the increased cell density in layer III. The border towards layer VI is barely recognizable, just like in area PF. The transition between layer VI and the white matter is not very sharp.

The fifth area of the rostral IPC is PFcm (Fig. 5). It lies in the depths of the parietal operculum, ventral to PF and caudal to PFop. The cortex of PFcm is narrower, and the cell density across all layers is lower than in either PF or PFm. Layer II is narrow but can be clearly separated from layer III. Large pyramids in lower layer III are a conspicuous feature of PFcm, as they are in PFt. Both areas differ also with respect to the columnar arrangement of the cell bodies. A distinct columnar arrangement is found in PFcm, extending from layer III through VI. Layer IV is sparsely developed. In layer V, there is no subdivision into upper and lower sub-layers. The layer VI/white matter border is very sharp.

The caudal IPC region begins occipital to PFm. It consists of two areas, a rostral (PGa) and a caudal (PGp) area.

In PGa (Fig. 6A), the very prominent layer IV is shifted to a more superficial position and subdivides the cortex into two equally wide bands, one above and one below layer IV. These are the general cytoarchitectonic features which separate the caudal from the rostral IPC region. Further characteristics of area PGa include a very narrow layer II, an abrupt increase in the sizes of pyramidal cells from superficial to deep layer III, a low cell density in layer V, a relatively dark layer VI (reflecting its higher cell

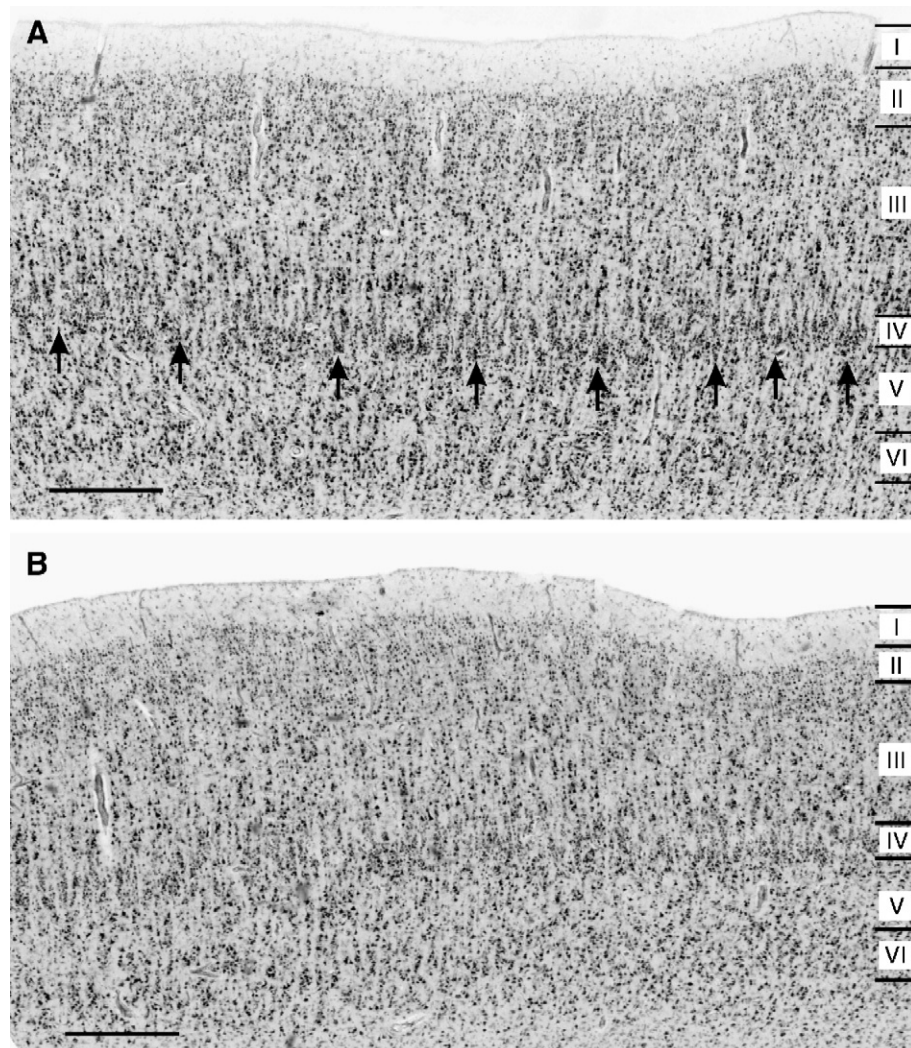


Fig. 4. (A) Cytoarchitectonic features of area PF. Strands of pyramidal cells extending from layer III into layer V are labeled by arrows. (B) Cytoarchitecture of area PFm. Roman numerals indicate cortical layers. Scale bar (A, B): 500 μ m.

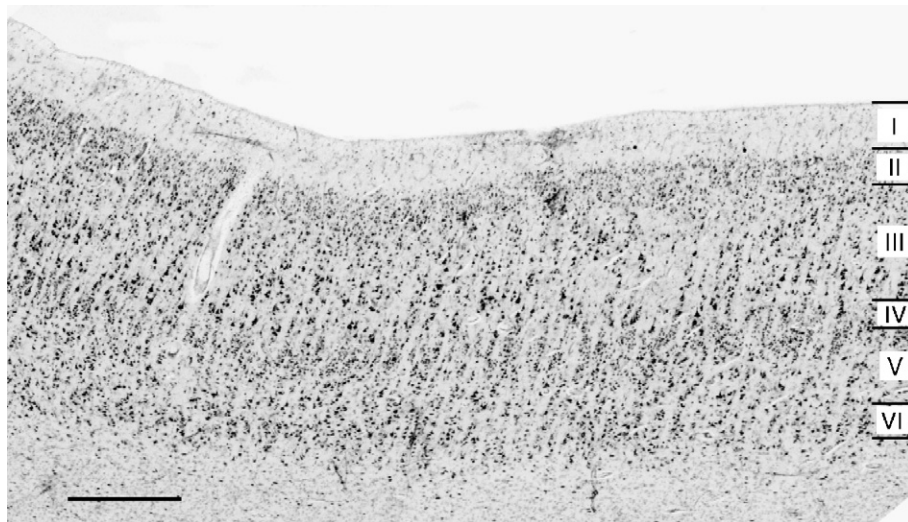


Fig. 5. Cytoarchitectonic features of area PFcm. A marked columnar arrangement is visible across layers III to VI. Roman numerals indicate cortical layers. Scale bar: 500 μ m.

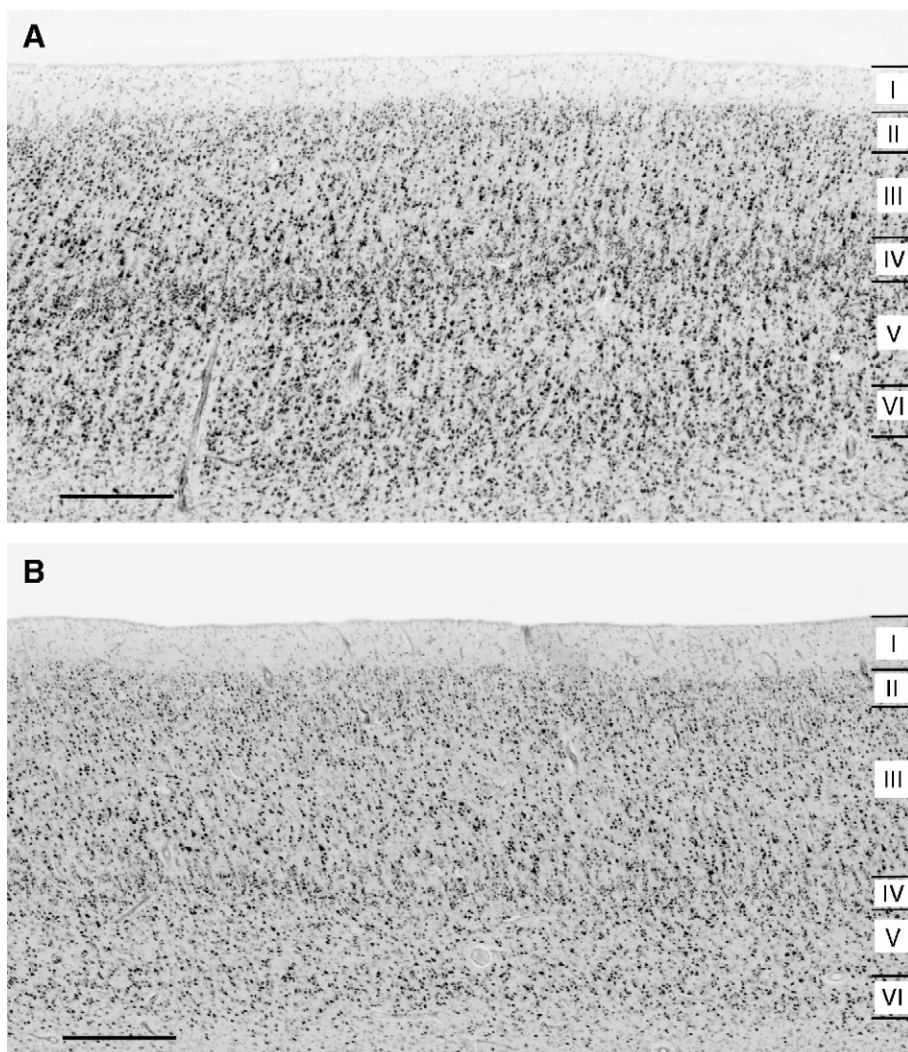


Fig. 6. (A) Cytoarchitectonic features of area PGa. (B) Cytoarchitectonic features of area PGp. Roman numerals indicate cortical layers. Scale bar (A, B): 500 μ m.

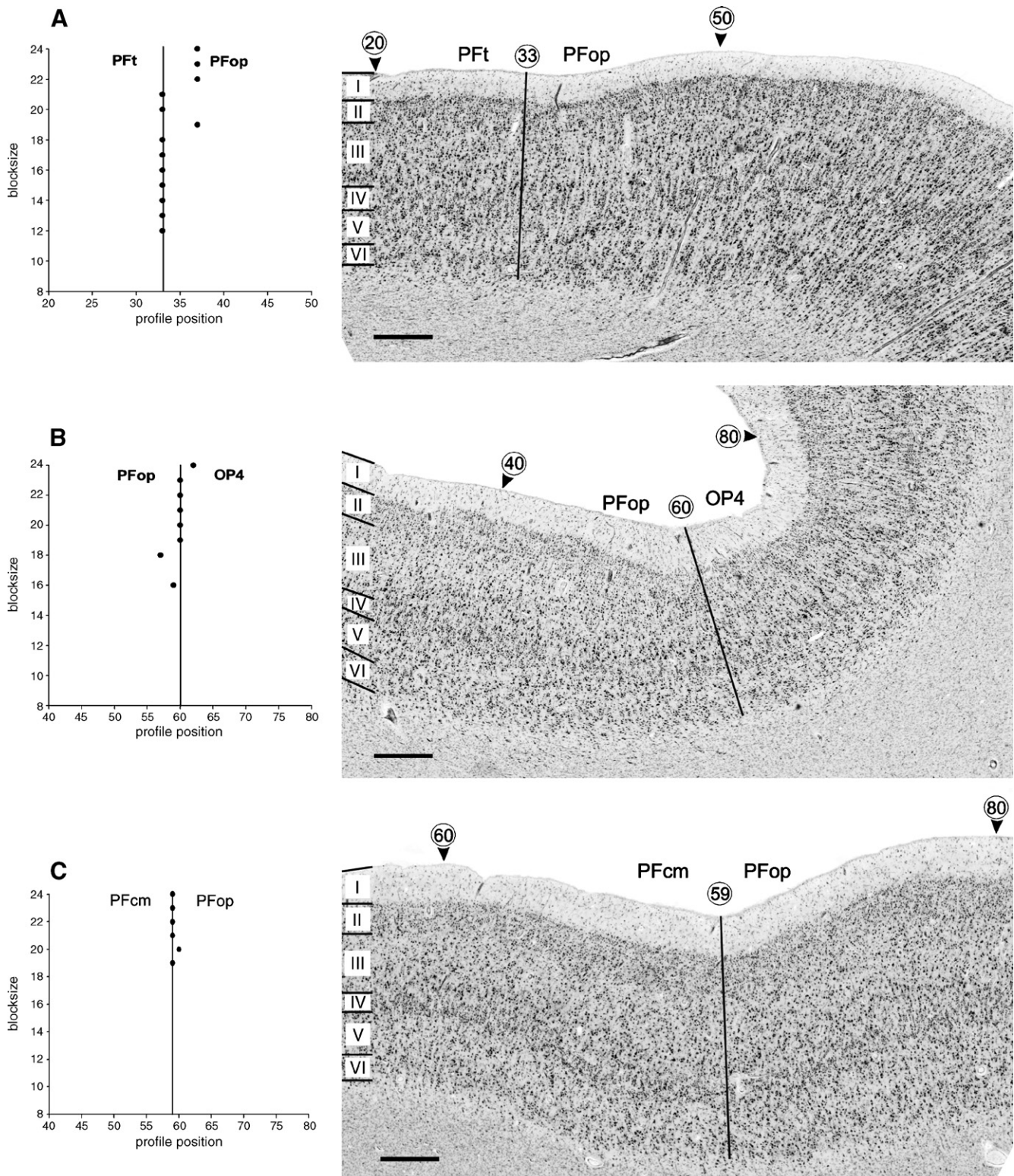


Fig. 7. (A) Border between area PFt and PFop. The significant ($p < 0.05$) maximum in the Mahalanobis plot at profile position no. 33 (left; vertical line) marks the cytoarchitectonic border (right; vertical line). (B) Border between area PFop and OP4 at profile position no. 60. (C) Border between PFop and area PFcm at profile position no. 59. Roman numerals indicate cortical layers, circled Arabic numerals indicate profile positions, arrowheads mark the starting- and end-points of the cortical sector covered by the Mahalanobis plot on the left side of each photomicrograph. For other conventions, see Fig. 2. Scale bar (A–C): 500 μ m.

density), which can be clearly separated from layer V, and an indistinct border between layer VI and the white matter.

The caudal area, PGp (Fig. 6B), has a slightly broader layer II than area PGa. Its granular cells intermingle with the small pyramids in upper layer III so that the border between layers II and III is difficult to identify. Layer III appears fairly homogeneous

with a minor superficial-to-deep increase in pyramidal cell size. Layer IV shifts to a deeper position in the cortex, making layer III wider than it is in PGa. As in PGa, layer IV is clearly visible. Layer V has a very low cell density and appears as a light stripe between the darker layers IV and VI. Cell density in layer VI is not as high as in PGa. The layer VI/white matter border is sharp.

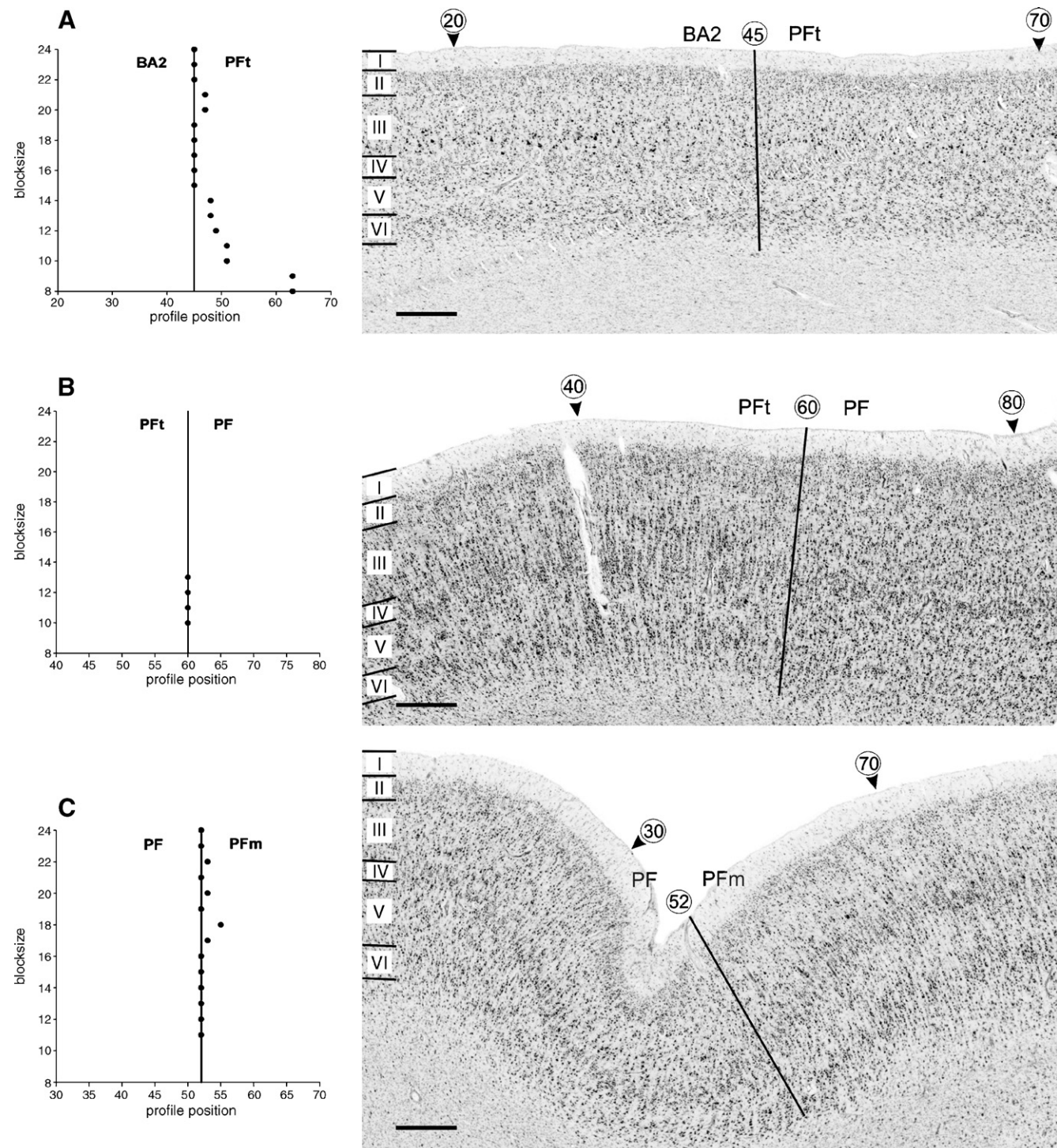


Fig. 8. (A) Border between area BA 2 and PFt at profile position no. 45. (B) Border between area PFt and PF at profile position no. 60. (C) Border between area PF and PFm at profile position no. 52. For other conventions, see Figs. 2 and 7. Scale bar (A–C): 500 μm.

Borders between the IPC areas

The rostralmost areas of the IPC are PFop and PFt. PFop is located on the dorsal shoulder of the lateral fissure between the

operculum Rolandi and the free surface of the IPC where it has a common border with area PFt (Fig. 7A). From PFt to PFop, the cortex becomes more homogeneous, larger pyramidal cells appear in layer V, layer VI becomes more cell dense, and the border

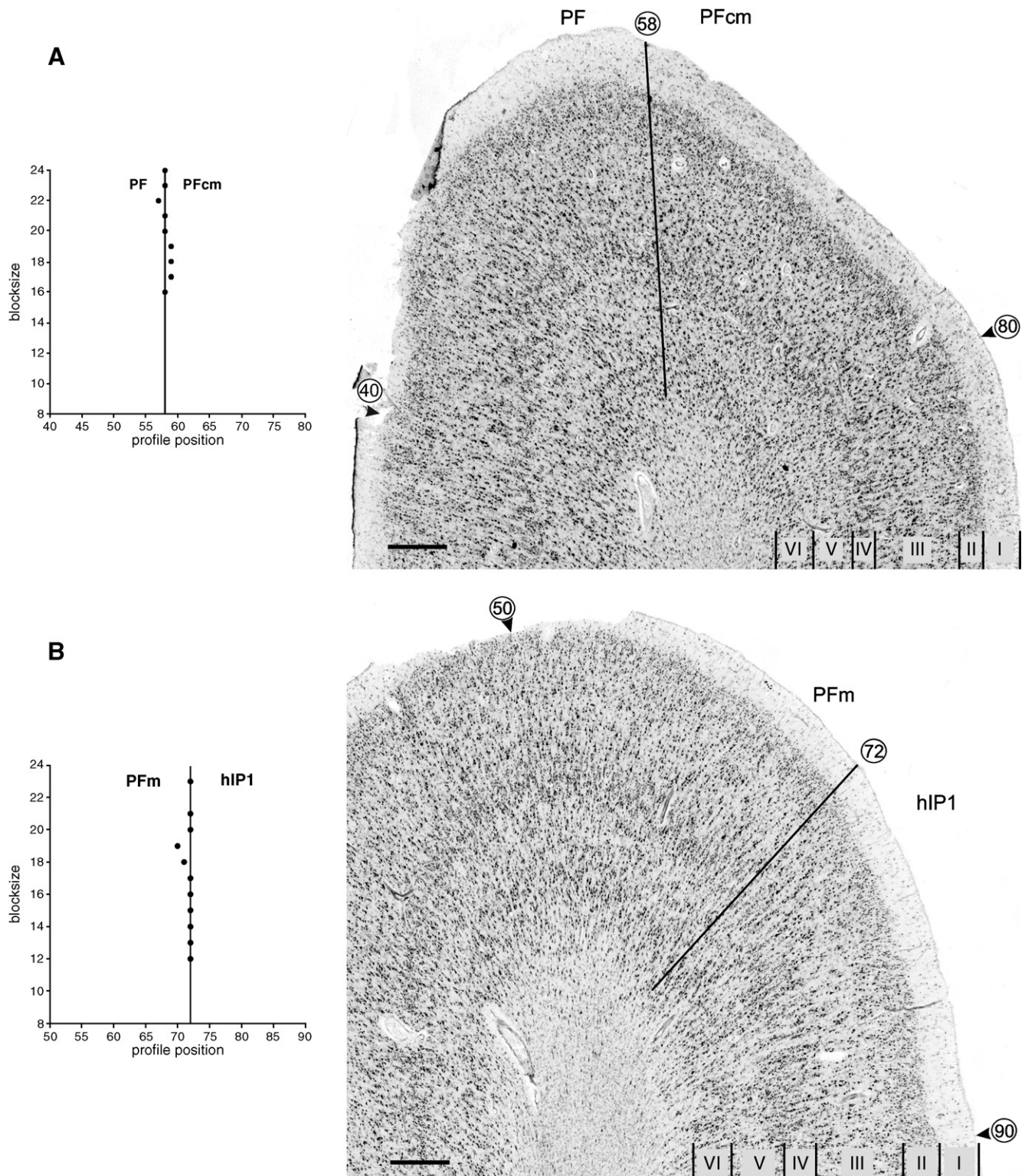


Fig. 9. (A) Border between area PF and PFcm at profile position no. 58. (B) Border between area PFm and hIP1 at profile position no. 72. For other conventions, see Figs. 2 and 7. Scale bar (A–C): 500 μ m.

between layer VI and the white matter becomes more blurred. PFop has a common border with area OP4 (Eickhoff et al., 2006a, b) of the parietal operculum (Fig. 7B). At the transition from PFop

to OP4, the cortex thickness decreases, the pyramidal cells in lower layer III increase in size, and a columnar arrangement of the cells in layers III to V becomes apparent. This border can be confirmed

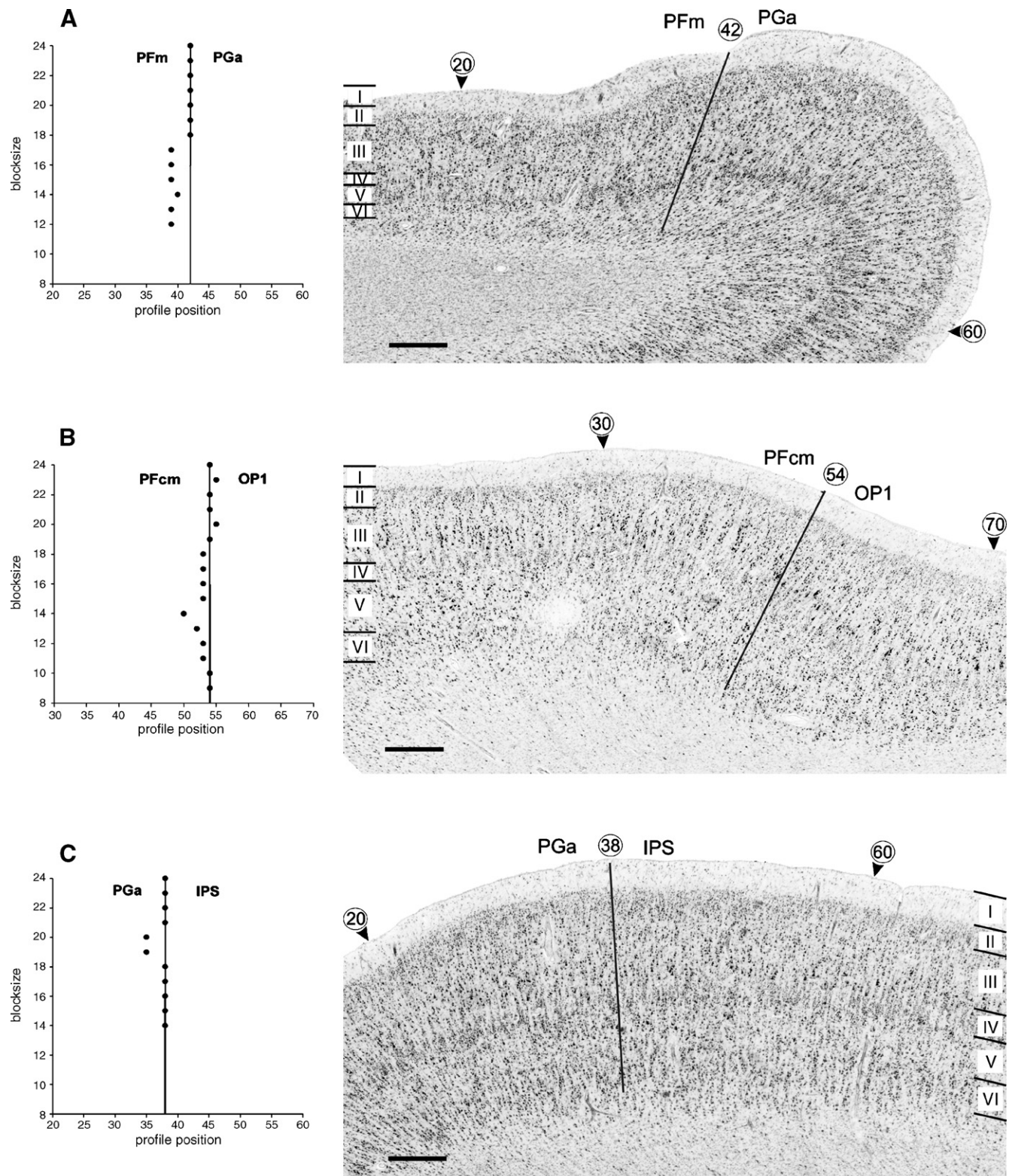


Fig. 10. (A) Border between area PFm and PGa at profile position no. 42. (B) Border between area PFcm and OP1 at profile position no. 54. (C) Border between area PGa and the cortex of the intraparietal sulcus (IPS) at profile position no. 38. For other conventions, see Figs. 2 and 7. Scale bar (A–C): 500 μm.

with the observer-independent technique and is found at profile position no. 60 in Fig. 7B. PFop also has a common border with caudally adjacent area PFcm (Fig. 7C). From PFop to PFcm, the cortex thins, the layers are more clearly separated, upper layer III lightens because of decreased cell packing density, and lower layer III has larger pyramidal cells. This border is confirmed at profile no. 59 (Fig. 7C).

Area PFt is a small region dorsal to PFop. PFt occupies the rostralmost sector of the IPC and separates it from somatosensory area BA 2 (Grefkes et al., 2001). BA 2 is characterized by big pyramids in lower layer III and a distinct layer V which appears light between the cell dense layers IV and VI. This transition is shown in Fig. 8A where the statistical method confirms the border at profile no. 45. The big pyramids in lower layer III of BA2 disappear in PFt, layer II becomes more cell dense, and larger layer V pyramidal cells are visible. Ventrally, PFt has a common border with PFop. Area PFt lies rostral to PF. The border between PFt and PF coincides with profile position no. 60 in Fig. 8B. In contrast to area PFt, the layers in PF are not clearly separable.

PF covers the major part of the supramarginal gyrus. When the rostro-caudal extent of the Sylvian fissure is short, area PF reaches to the superior temporal gyrus. PF is surrounded by PFt rostrally, PFcm ventrally, and PFm caudally. The border between PF and

PFm (Fig. 8C) does not correlate with macroanatomical landmarks. The observer-independent algorithm detects this border at profile position no. 52. From PF to PFm, the separation of the layers becomes more obvious, layer IV more pronounced, layer V lighter, and the overall cell packing is denser.

The border between PF and PFcm is shown in Fig. 9A. In most hemispheres, this border is found at the shoulder of the parietal operculum. The cortex of PFcm narrows, the contrast between layer IV and its adjacent layers III and V increases, and layer V becomes lighter (cf. profile position no. 58).

Area PFm abuts rostrally on PF (see above), dorsally on the ventral intraparietal (hIP1; Choi et al., 2006) area in the intraparietal sulcus (IPS), and caudally on PGa. The transition between PFm and hIP1 can be found in Fig. 9B at position no. 72. Across this border, overall cell density decreases and layers III through V become lighter. In hIP1, medium-sized pyramids are in lower layer III, whereas upper layer III is cell sparse.

The most important border in the IPC is the transition between its rostral and caudal part, i.e., the transition between area PFm and PGa (Fig. 10A). This position (no. 42) coincides with obvious changes in cytoarchitecture. From PFm to PGa, layer IV becomes more prominent and shifts from the deepest third to the middle of the cortical width. Furthermore, in layer III, there is a sudden

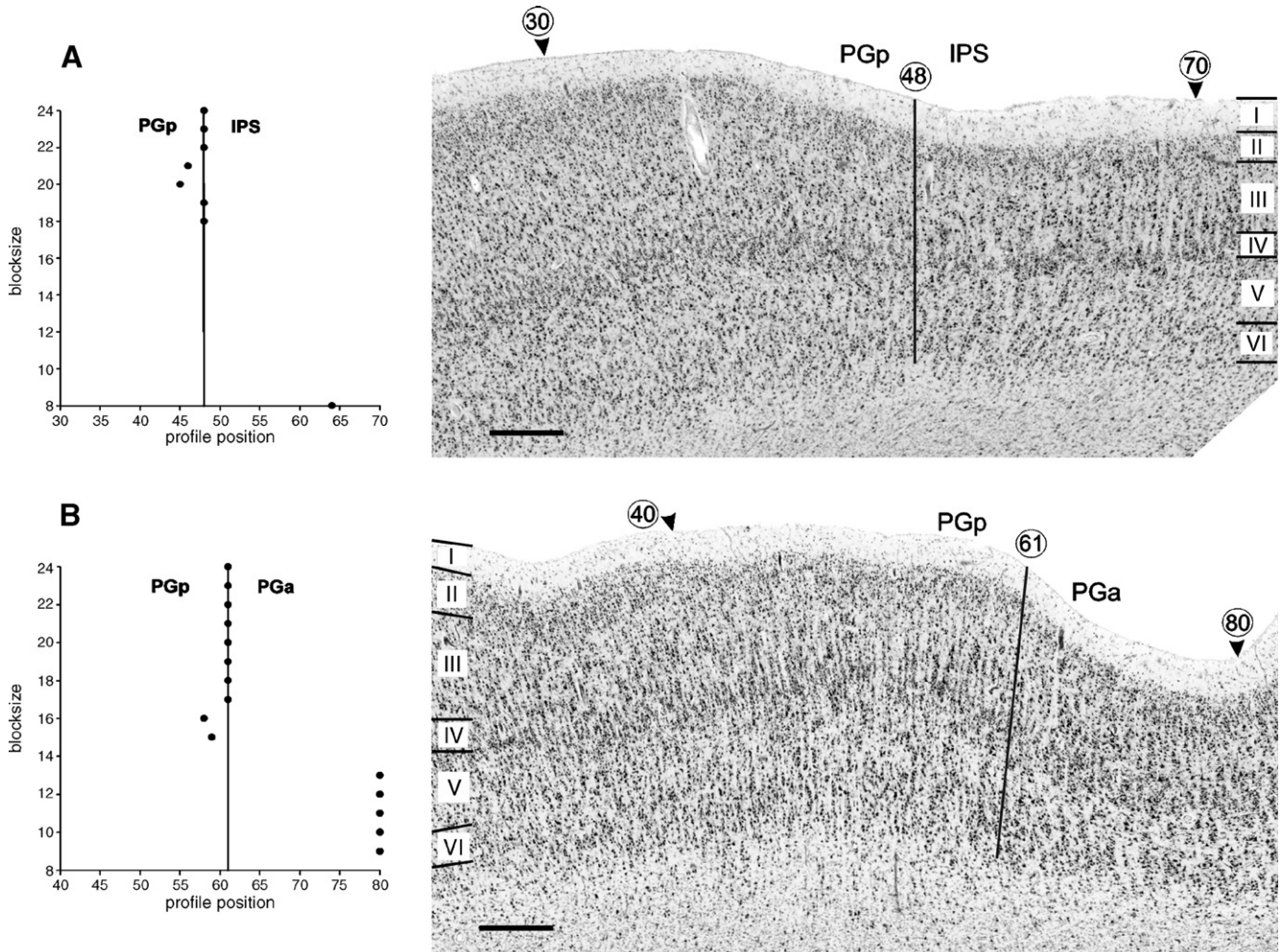


Fig. 11. (A) Border between area PGp and IPS at profile position no. 48. (B) Border between area PGp and PGa at profile position no. 61. For other conventions, see Figs. 2 and 7. Scale bar (A, B): 500 μm.

increase in cell size between its upper and lower part. There is no macroanatomical structure that can be used as an approximate landmark for this border.

The most caudo-ventral region of the rostral IPC, area PFcm, is surrounded dorsally by PF, rostrally by PFop, and medially by OP1

(Eickhoff et al., 2006a,b). The borders with PFop and PF have been described above. The border between PFcm and OP1 is shown in Fig. 10B. The observer-independent algorithm detects this border at profile position no. 54 which coincides with visible changes in microstructure. The cortex of OP1 is thicker and

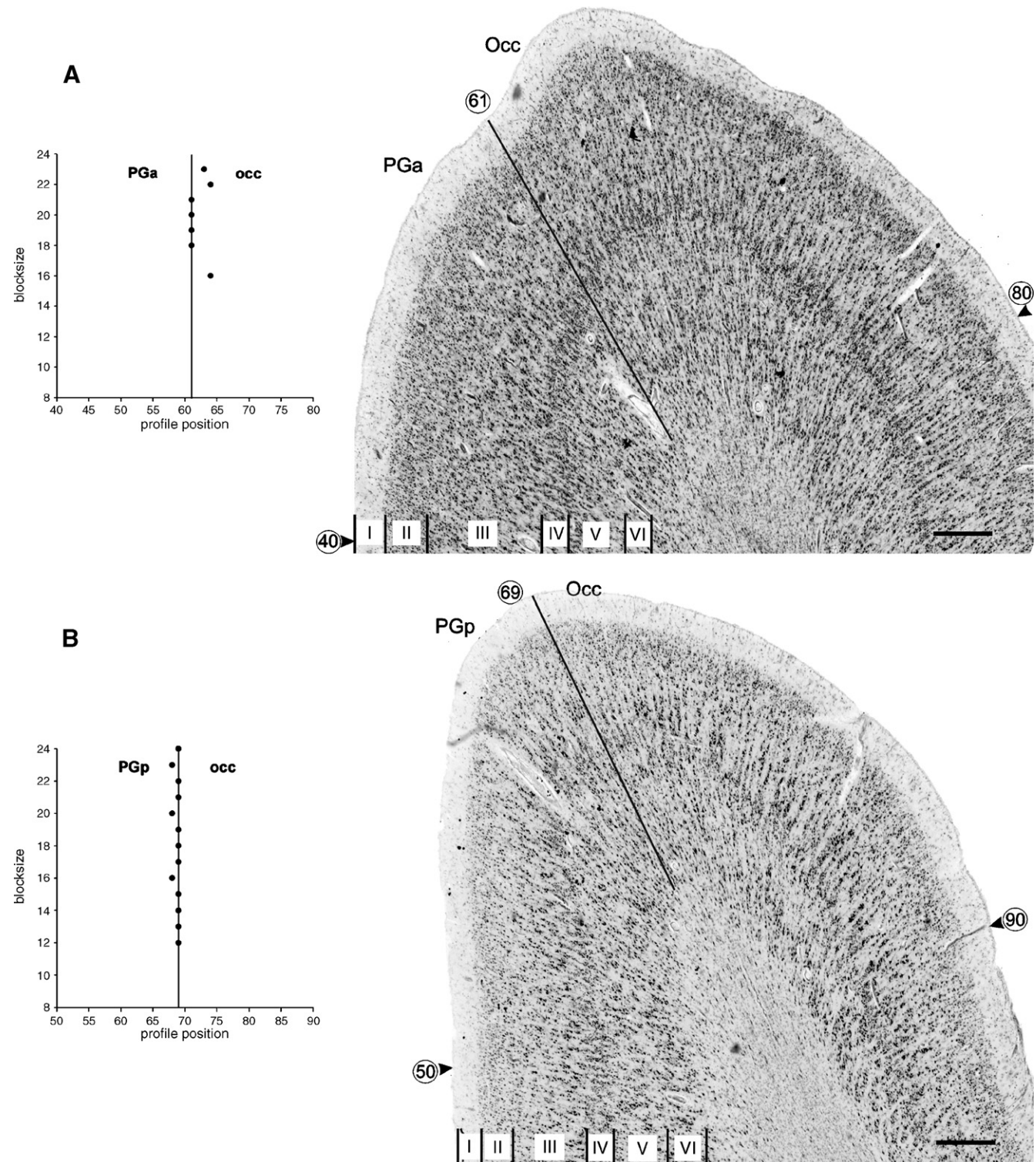


Fig. 12. (A) Border between area PGa and the occipital cortex (Occ) at profile position no. 61. (B) Border between area PGp and the Occ at profile position no. 69. For other conventions, see Figs. 2 and 7. Scale bar (A–B): 500 μm.

contains larger layer IIIc pyramids than PGp. This border lies in the depth of the parietal operculum between its middle and innermost (towards the insula) third.

Area PGa and PGp have common borders with the cortical areas of the intraparietal sulcus (IPS) dorsally and the occipital lobe ventrally. The PGa/IPS and PGp/IPS borders are shown in Figs. 10C and 11A, respectively. In Fig. 10C, profile position no. 38 indicates the border between PGa and the IPS cortex. Layer V is lighter in IPS than in PGa. In Fig. 11A, profile position no. 48 indicates the border between PGp and the IPS. The cortex of IPS narrows and the cells of layer III increase in size. In most brains, these two borders are located at or close to the lateral shoulder of the IPS. In some cases, particularly regarding the PGa/IPS transition, the border is also found on the free cortical surface, particularly when the IPS consists of two separated branches.

The border between the two areas of the caudal IPC, areas PGa and PGp, is shown in Fig. 11B. The border at profile position no. 61 coincides with obvious cytoarchitectonic changes. In PGp, the cells in all layers are smaller than those in PGa, and layer V appears lighter in PGa than PGp. This border is located in the angular

sulcus which is the continuation of the superior temporal sulcus into the caudal part of the IPC.

The transitions between PGa and PGp and the occipital lobe (Occ) are shown in Figs. 12A and B, respectively. The cortex of Occ is relatively narrower and has larger pyramidal cells than PGp in lower layer III and layer V. These differences in pyramidal cell sizes are more pronounced at the border with PGp than with PGa. The large pyramids of layer III are characteristic for the “occipital cortex” type as described by von Economo and Koskinas (1925). These observations are confirmed by the observer-independent algorithm (PGa/Occ border at profile position no. 61 (Fig. 12A) and PGp/Occ border at profile position no. 69 (Fig. 12B)).

As an example, Fig. 13 shows the parcellation of the anterior IPC in eleven coronal MRI sections through a right hemisphere of the same brain as used in Figs. 2–12. The areas of the anterior IPC (correspondent to BA 40) as well as adjacent areas like OP1, and OP2 (Eickhoff et al., 2006a,b), BA2 (Grefkes et al., 2001) and hIP2 (Choi et al., 2006) extend into prominent sulci like the postcentral (poc), intraparietal sulcus (ips) and the Sylvian fissure (Sf).

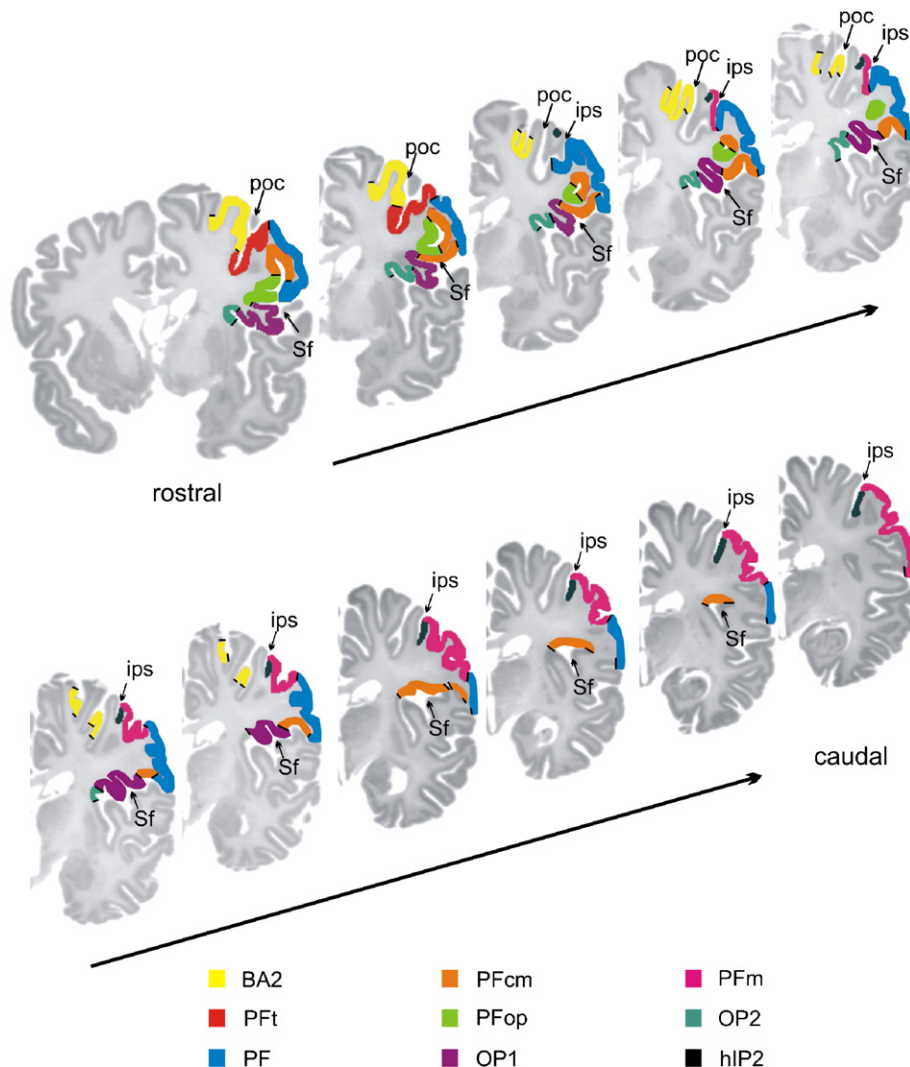


Fig. 13. A rostro-caudal sequence of eleven coronal MRI sections through the right hemisphere of the same brain as shown in Figs. 2–12). The different anterior IPC areas (PFop, PFcm, PF, PFt, PFm) and adjacent areas (OP2, OP1, BA2, hIP2) are labeled in different colors. poc, postcentral sulcus, ips, intraparietal sulcus, Sf, Sylvian fissure. Distance between sections: 1.2 mm.

Topographical variability of the IPC areas

To display each area's topography on the cortex, we reconstructed the ten brains in 3-D and rendered the IPC areas on the cortical surfaces of the brains. Specifically, we wanted to know whether the IPC areas have a consistent topographical arrangement, and if so, to what extent the arrangement varies between hemispheres and brains.

Fig. 14 shows as representative examples the parietal part of five brains (left and right lateral views). In all ten brains, the cytoarchitectonic areas are arranged in a topologically comparable pattern; i.e., in two parallel rostro-caudal sequences: three dorsal areas (PFt, PF, and PFm) and two smaller ventral areas (PFop and PFcm). PGa and PGp are found farther caudally (corresponding to the approximate position of BA 39). Again, a consistent pattern is obvious: PGa occupies always the rostral and PGp the caudal part of BA 39.

However, we also noticed variations in position and extent of the areas both between individuals and between hemispheres of the

same brain. A striking example is area PFcm. In most cases, it is found in the upper bank of the Sylvian fissure. In some brains (e.g., in **Fig. 14A**, right hemisphere, and B, both hemispheres), however, PFcm extends onto the free surface of the parietal operculum. Alternatively (e.g., **Fig. 14A**, left hemisphere), PFcm is entirely buried in the depths of the Sylvian fissure and not visible on the exposed parietal surface. Another example is the ventral border of area PF with the superior temporal gyrus. In some cases (e.g., **Figs. 14A** and B, right hemispheres), the ventral part of PF occupies the caudal end of the superior temporal gyrus, whereas in other cases (e.g., **Figs. 14C** and D, left hemispheres), it does not.

No macroanatomical landmark reliably marks a cytoarchitectonic border between any of the IPC areas.

Discussion

The IPC was repeatedly parcellated during the last century (Bailey and von Bonin, 1951; Batsch, 1956; Brodmann, 1909; Campbell, 1905; Gerhardt, 1940; Sarkissov et al., 1955; Vogt

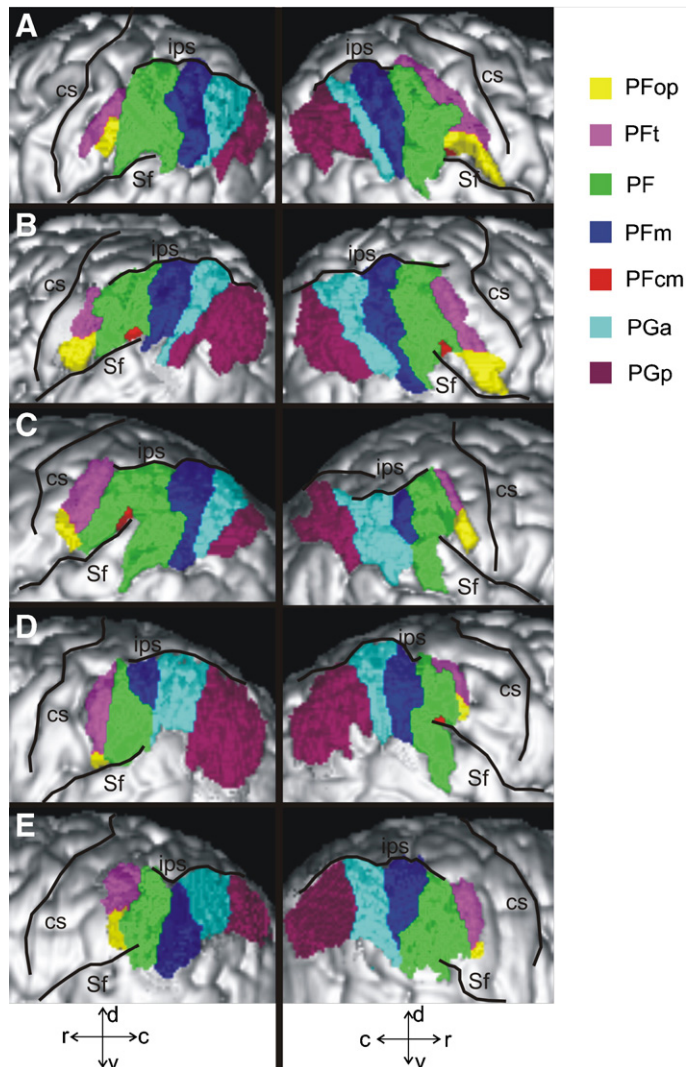


Fig. 14. Intersubject variability of the IPC. 3-D reconstructions of five out of the ten human brains studied demonstrate this variability in size and extent. Left hemispheres are shown in the left column, right hemispheres in the right column. Area PFcm is not visible in all hemispheres from lateral viewpoint because major parts of it are hidden in the Sylvian fissure. Note that there is no correspondence between macroanatomical landmarks and cytoarchitectonic borders. c: caudal direction, d: dorsal direction, r: rostral direction, v: ventral direction, Sf: Sylvian fissure, cs: central sulcus, ips: intraparietal sulcus.

and Vogt, 1919; von Economo and Koskinas, 1925). Each map, however, is a schematic drawing of the macro- and micro-anatomical topography of only one brain, and each investigator employed criteria for defining borders between different cortical areas, which are dependent on the experience and pattern recognition capabilities of the observer. This produced IPC maps that differ from each other in many aspects.

Using a reproducible observer-independent methodology, we produced a new IPC map that accounts for interindividual variability, avoids non-testable judgments about microstructural borders, and produces a 3-D registered map, which can be aligned with data from functional imaging studies.

Cytoarchitecture of the IPC

Brodmann (1909) described two areas in the IPC: rostral BA 40 on the supramarginal gyrus and caudal BA 39 on the angular gyrus. According to Brodmann, BA 40 reaches rostro-caudally from somatosensory area BA 2 to the Jenssen sulcus (primary intermediate sulcus). Using the Jenssen sulcus as a border between BA 40 and BA 39, we cannot support this finding because the presence of this sulcus is highly variable. When the primary intermediate sulcus is present, the transition between PFm and PGa lies in its depth. In all other cases, the transition is either on the free cortical surface or in the depth of an unnamed sulcus, which cannot be identified as Jenssen sulcus according to Ono et al. (1990).

Dorsal-ventrally BA 40 reaches from the IPS into the depths of the parietal operculum towards the insular cortex. Opercular parts of BA 40 are, however, covered by areas OP1 and OP2 (Eickhoff et al., 2006a,b). The remaining opercular sector of BA 40 matches our areas PFop and PFcm. PFop is found between the rostral operculum and the free IPC surface. PFcm lies in the caudal operculum and extends from the insula and retroinsular region to the free IPC surface. The free IPC surface of BA 40 coincides with our areas PFt, PF, and PFm (taking into account that the Jenssen sulcus cannot be found in every brain).

Caudal to area PFm, the cytoarchitecture changes, indicating the appearance of BA 39, which correlates with our areas PGa and PGp. PGa and PGp extend from the IPS to the temporo-occipital junction (PGa) and from the IPS to the occipital lobe (PGp).

von Economo and Koskinas (1925) segregated six areas in their detailed description of the IPC. Five of the six areas approximately match the position of BA 40, the sixth area coincides roughly with a rostral part of BA 39. Our map is more similar to the map of von Economo and Koskinas (1925) than that of Brodmann (1909). We found a set of seven areas in the IPC: five areas are located approximately in the region of BA 40 and are roughly comparable with areas PFop, PFt, PF, PFm and PFcm of von Economo and Koskinas (1925). In contrast to von Economo and Koskinas, we found two areas in BA 39, i.e., PGa and PGp.

von Economo and Koskinas (1925) described area PFt as a narrow cortical band with light layers III and V, well developed layers IV and VI, and a discrete columnar arrangement of the cells (more pronounced on the free cortical surface, less so in the walls of the sulci). These cytoarchitectonic features as well as the localization as the most rostro-dorsal region of the IPC fit well with our observations.

Area PFop is not described explicitly by von Economo and Koskinas (1925). They mention only that PFop is similar to PFt and extends onto the operculum Rolandi. PFop, as we define it,

only partially overlaps with the similarly named PFop of von Economo and Koskinas (1925) and is the caudo-lateral part of their PFop. The rest is opercular cortex, OP1–OP3 (Eickhoff et al., 2006a,b). As the cytoarchitecture of our area PFop differs from that of PFt, we define PFop as a separate region.

Area PF is the main rostral IPC region in the von Economo and Koskinas (1925) map. Its prominent cytoarchitectonic features are the rather homogeneous size and distribution of the cells with a fine columnar arrangement, small cells in all layers, a superficial-to-deep increase in the size of the pyramids in layer III, and well developed layers II and IV. We corroborated these criteria as well as von Economo's and Koskinas's observation that area PF is very large and its ventral part reaches to the superior temporal gyrus.

von Economo's and Koskinas's area PFm has larger pyramidal cells in deep layer III and lies caudal to area PF. We could corroborate these observations but found additional cytoarchitectonic features which are characteristic for area PFm like the well developed layer IV and its light layer V in contrast to PF.

Likewise, we corroborated von Economo's and Koskinas's cytoarchitectonic description of area PFcm: large pyramids in lower layer III and a clear columnar arrangement of the cells. The topography of PFcm in their study and ours differs, however. The map of von Economo and Koskinas (Figs. 1C and D) shows PFcm caudal to the Sylvian fissure, where the supramarginal gyrus transitions to the superior temporal gyrus. We found PFcm in the caudal part of the operculum Rolandi, i.e., in the depths of the Sylvian fissure.

In the caudal IPC, von Economo and Koskinas defined only one region, area PG. Its main characteristics are a small cortical width and relatively narrow layers II and III, medium-sized pyramids in lower layer III, a wide and well developed layer IV, and a light layer V. This description fits with our area PGa. In addition, however, we defined an area caudal to PGa, which we termed area PGp.

Taken together, von Economo and Koskinas defined two main areas in the IPC: PF rostrally and PG caudally. They considered the other regions (PFt, PFop, PFcm, and PFm) – as the nomenclature suggests – to be regional variants of area PF (area PG was not subdivided any further) and did not provide any clear-cut borders between them. We describe distinct areas (each with its own characteristic features) with clear-cut borders between them (which were confirmed with an observer-independent method). The IPC areas have main characteristic features in common by which they can be distinguished from surrounding areas. It can be stated as well that some IPC areas have more cytoarchitectonic features in common than others (which need not necessarily be anatomically adjacent areas).

Vogt and Vogt (1919) studied the myeloarchitecture of IPC. They found three areas on the free surface of the IPC (88, 89, and 90) and two areas in the caudal part of the operculum (73 and 74) (cf. Fig. 1B). The position of area 88, which also extends into the rostral part of the operculum Rolandi, may correlate with our areas PFt and PFop. Area 89, the main region on the free surface of the IPC, is comparable to our PF. Like PF, area 89 also extends into the depth of the parietal operculum. Area 90 most likely corresponds to von Economo's and Koskinas's area PG, which is represented by our areas PGa and PGp. A possible correlate of our PFcm could be area 74 and that part of area 73 lying in the caudalmost parietal operculum that does not extend onto the free surface of the IPC.

A similar arrangement of areas with the same nomenclature was published by [Batsch \(1956\)](#), who performed myeloarchitectonic observations in IPC. Minor differences to the map of [Vogt and Vogt \(1919\)](#) can be found.

[Gerhardt \(1940\)](#) published a cytoarchitectonic map very similar to the myeloarchitectonic maps of [Vogt and Vogt \(1919\)](#) and [Batsch \(1956\)](#). In contrast to Vogt and Vogt, her area 88 has a somewhat larger extension on the free surface of the IPC and does not extend into the operculum, and her area 74 lies mainly in the operculum Rolandi but also extends onto the free surface of the IPC. Area 88 is followed caudally by areas 89 and 90, which have a comparable extension on the IPC surface. Thus, our parcellation is similar to the maps of both [Vogt and Vogt \(1919\)](#) and [Gerhardt \(1940\)](#).

In a cytoarchitectonic study, [Sarkissov et al. \(1955\)](#) followed [Brodmann's \(1909\)](#) scheme of the IPC regarding the principal subdivision into two areas (40 rostrally and 39 caudally), but described also several subdivisions within each area (cf. Fig. 1E). Some of them, like 40op and 40p/40i, may be comparable with our areas PFop and PFm, respectively. In the caudal IPC, a straightforward correlation between their areas 39, 39s, and 39p and our areas PGa and PGp cannot be reliably established. The cytoarchitecture of the subdivisions 39s and 39p of [Sarkissov et al. \(1955\)](#) is similar to their area 39, but exhibits also some similarities to the adjacent areas ([Sarkissov et al., 1949](#)). 39p could at least be a part of our PGp since [Sarkissov et al. \(1949\)](#) described it to be the most posterior part of caudal IPC. However, we could not corroborate their description of this area. The other area, 39s, was not found in our study. These differences between our map and the map of [Sarkissov et al. \(1955\)](#) may be caused by the fact that they defined architectonic borders in only two brains by pure visual inspection, whereas a quantitative, statistically testable and observer-independent approach was used in the present observations.

Topographical intersubject and left-right variability

We found considerable variability between different individuals as well as between left and right hemisphere of the same subject. The variability involved both the topographic location of borders and the asymmetry in size of a cortical area.

Important sulci surrounding the IPC are the intraparietal sulcus (IPS), the Sylvian fissure, and the postcentral sulcus. In our sample, especially the IPS and the Sylvian fissure showed an especially high variability. The rostro-caudal extent and the progression of the horizontal and ascending branches of the Sylvian fissure varied between different brains and between left and right hemispheres. The IPS differed between the brains in its rostral starting point and its rostro-caudal continuity. In some of our brains, the IPS consisted of two or three parts that were separated from each other by a gyrus. These findings fit well with former reports, e.g., of [Ono et al. \(1990\)](#).

This variability of sulcal patterns may explain some of the topographical variability of the IPC areas. In hemispheres with a short Sylvian fissure, area PF can encroach on the superior temporal gyrus, as seen in Figs. 13B and C. The presence or absence of small sulci within the IPC, for example, the Jenssen sulcus, adds to the observed variability. Gyral patterns also differ remarkably between hemispheres and brains. The macroanatomical gyral landmarks of the IPC are the supramarginal gyrus (BA 40) and the angular gyrus (BA 39). Differences in their size and shape are associated with variability of size and shape in the IPC areas.

These findings explain partly the considerable variability of the IPC areas. There are two classes of variability: class 1 variability is not predictable from macroscopical landmarks; in contrast to that, class 2 variability is predictable from visible landmarks. As described by [Rademacher et al. \(1993\)](#), class 2 variability is found in primary cortical areas. In the present study, class 1 variability seems to be relevant since the cytoarchitectonic borders between the IPC areas and adjacent areas cannot be located by macroanatomical landmarks. The same cytoarchitectonic border, e.g., the border between areas PF and PFm, can be found on top of a gyrus, near the transition from gyrus to sulcus or in the depth of the sulcus.

Acknowledgments

The authors thank U. Blohm for excellent histological work. This work was supported by a grant (to K.Z.) funded by the DFG (grant KFO 112), a Human Brain Project/Neuroinformatics Research grant funded by the National Institute of Biomedical Imaging and Bioengineering, the National Institute of Neurological Disorders and Stroke, and the National Institute of Mental Health and by a grant (to K.Z.) of the European Commission (Grant QLG3-CT-2002-00746).

References

- Amunts, K., Schleicher, A., Bürgel, U., Mohlberg, H., Uylings, H.B.M., Zilles, K., 1999. Broca's region revisited: cytoarchitecture and intersubject variability. *J. Comp. Neurol.* 412, 319–341.
- Amunts, K., Malikovic, A., Mohlberg, H., Schormann, T., Zilles, K., 2000. Brodmann's areas 17 and 18 brought into stereotaxic space—Where and how variable? *NeuroImage* 11, 66–84.
- Bailey, P., von Bonin, G., 1951. The Isocortex of Man. University of Illinois Press, Urbana, IL.
- Batsch, E.G., 1956. Die myeloarchitektonische Untergliederung des Isocortex parietalis beim Menschen. *J. Hirnforsch.* 2, 225–258.
- Brodmann, K., 1909. Vergleichende Lokalisationslehre der Großhirnrinde. Barth, Leipzig.
- Campbell, A.W., 1905. Histological Studies on the Localization of Cerebral Function. University Press, Cambridge.
- Choi, H.J., Zilles, K., Mohlberg, H., Schleicher, A., Fink, G.R., Armstrong, E., Amunts, K., 2006. Cytoarchitectonic identification and probabilistic mapping of two distinct areas within the anterior ventral bank of the human intraparietal sulcus. *J. Comp. Neurol.* 495, 53–69.
- Eickhoff, S.B., Stephan, K.E., Mohlberg, H., Grefkes, C., Fink, G.R., Amunts, K., Zilles, K., 2005. A new SPM toolbox for combining probabilistic cytoarchitectonic maps and functional imaging data. *NeuroImage* 25, 1325–1335.
- Eickhoff, S., Schleicher, A., Zilles, K., Amunts, K., 2006a. The human parietal operculum: I. Cytoarchitectonic mapping of subdivisions. *Cereb. Cortex* 16, 254–267.
- Eickhoff, S., Amunts, K., Mohlberg, H., Zilles, K., 2006b. The human parietal operculum. II. Stereotaxic maps and correlation with functional imaging results. *Cereb. Cortex* 16, 268–279.
- Gerhardt, E., 1940. Die Cytoarchitektonik des Isocortex parietalis beim Menschen. *J. Psychol. Neurol.* 49, 367–419.
- Geyer, S., 2004. The microstructural border between the motor and the cognitive domain in the human cerebral cortex. Advances in Anatomy Embryology and Cell Biology, vol. 174. Springer, Berlin.
- Geyer, S., Ledberg, A., Schleicher, A., Kinomura, S., Schormann, T., Bürgel, U., Klingberg, T., Larsson, J., Zilles, K., Roland, P.E., 1996. Two different areas within the primary motor cortex of man. *Nature* 382, 805–807.
- Geyer, S., Schleicher, A., Zilles, K., 1999. Areas 3a, 3b, and 1 of human

- primary somatosensory cortex: 1. Microstructural organization and interindividual variability. *NeuroImage* 10, 63–83.
- Grefkes, C., Geyer, S., Schormann, T., Roland, P., Zilles, K., 2001. Human somatosensory area 2: observer-independent cytoarchitectonic mapping, interindividual variability, and population map. *NeuroImage* 14, 617–631.
- Jones, S.E., Buchbinder, B.R., Aharon, I., 2000. Three-dimensional mapping of cortical thickness using Laplace's equation. *Hum. Brain Mapp.* 11, 12–32.
- Mahalanobis, P.C., Majumda, D.N., Rao, C.R., 1949. Anthropometric survey of the united provinces. A statistical study. *Sankhya* 9, 89–324.
- Merker, B., 1983. Silver staining of cell bodies by means of physical development. *J. Neurosci. Methods* 9, 235–241.
- Morosan, P., Rademacher, J., Schleicher, A., Amunts, K., Schormann, T., Zilles, K., 2001. Human primary auditory cortex: cytoarchitectonic subdivisions and mapping into a spatial reference system. *NeuroImage* 13, 684–701.
- Ono, M., Kubik, S., Abernathey, C.D., 1990. *Atlas of the Cerebral Sulci*. Thieme, Stuttgart/New York.
- Rademacher, J., Caviness, J., Steinmetz, H., Galaburda, A.M., 1993. Topographical variation of the human primary cortices: implications for neuroimaging, brain mapping, and neurobiology. *Cereb. Cortex* 3, 313–329.
- Sarkissov, S.A., Filimonoff, I.N., Preobrashenskaya, N.S., 1949. *Cytoarchitecture of the Human Cortex Cerebri (Russ.)*. Medgiz, Moscow.
- Sarkissov, S.A., Filimonoff, I.N., Kononowa, E.P., Preobraschenskaja, I.S., Kukuew, L.A., 1955. *Atlas of the Cytoarchitectonics of the Human Cerebral Cortex*. Medgiz, Moscow.
- Schleicher, A., Zilles, K., 1990. A quantitative approach to cytoarchitectonics: analysis of structural inhomogeneities in nervous tissue using an image analyser. *J. Microsc.* 157, 367–381.
- Schleicher, A., Amunts, K., Geyer, S., Morosan, P., Zilles, K., 1999. Observer-independent method for microstructural parcellation of cerebral cortex: a quantitative approach to cytoarchitectonics. *NeuroImage* 9, 165–177.
- Schmitt, O., Böhme, M., 2002. A robust transcranial profile scanner for generating 2-D traverses in histological sections of richly curved cortical courses. *NeuroImage* 16, 1103–1119.
- Schmitt, O., Böhme, M., 2003. Erratum to a robust transcranial profile scanner for generating 2-D traverses in histological sections of richly curved cortical courses. *NeuroImage* 18 (3), 811.
- Schormann, T., Zilles, K., 1998. Three-dimensional linear and nonlinear transformations: an integration of light microscopical and MRI data. *Hum. Brain Mapp.* 6, 339–347.
- Vogt, C., Vogt, O., 1919. Allgemeine Ergebnisse unserer Hirnforschung. *J. Psychol. Neurol.* 25, 279–461.
- von Economo, K., Koskinas, G., 1925. *Die Cytoarchitektonik der Hirnrinde des erwachsenen Menschen*. Springer, Wien.
- Zilles, K., Schleicher, A., Palomero-Gallagher, N., Amunts, K., 2002. Quantitative analysis of cyto- and receptorarchitecture of the human brain. In: Toga, A.W., Mazziotta, J.C. (Eds.), *Brain Mapping: The Methods*, 2nd ed. Academic Press, pp. 573–602.